scientific reports

Check for updates

OPEN

Green synthesis of zinc oxide nanoparticles using *Enterobacter cloacae* microorganism and their application in enhanced oil recovery

Mohammad Hossein Shabani[1], Arezou Jafari[1]✉, Mehrdad Manteghian[1]✉ & Seyyed Mohammad Mousavi[2,3]

Employing safe and inexpensive methods for the synthesis of biocompatible nanoparticles (NPs) can be very challenging. Green synthesis refers to the process of synthesizing nanoparticles without using toxic and dangerous chemicals. One of the applications of nanoparticles is increasing production from oil reservoirs, known as enhanced oil recovery (EOR). The main aim of the current study is the biosynthesis of zinc oxide (ZnO) nanoparticles (NPs) using *Enterobacter cloacae* (Persian Type Culture Collection (PTCC): 1798) microorganism, extracted from the formation water of one of the southwestern Iranian reservoirs, as a novel approach in EOR applications. Several analytical methods, including Fourier transform infrared (FTIR), field emission scanning electron microscope (FSEM), X-ray diffraction (XRD), dynamic light scattering (DLS), energy dispersive X-ray spectroscopy (EDS), and zeta potential were used to analyze the produced NPs. The FESEM analysis confirmed the amorphous form of the nanoparticles and estimated their size in the range of 32 to 58 nm. In investigating the effect of synthesized nanoparticles on interfacial tension (IFT) and stability tests, three levels of base fluids (distilled water, seawater, and diluted sea water) and five levels of nanoparticle concentrations (0, 100, 500, 1000, and 2000 ppm) were considered. The IFT analysis showed that an increase in nanoparticle concentration causes a decrease in the IFT. Also, ZnO nanoparticles were chosen at concentrations of 500 and 1000 ppm for wettability alteration and the EOR test through injection into porous media. The results for the EOR test demonstrated a maximum oil recovery factor of 56% for nanofluid injection with a concentration of 1000 ppm with diluted seawater as the base fluid. Furthermore, oil recovery factors of 43% and 49% were achieved by injection of distilled water and seawater with a concentration of 1000 ppm, respectively.

Keywords BioSynthesis, ZnO, Nanoparticle, Wettability, EOR, IFT

Abbreviations

API	American Petroleum Institute
NPs	Nanoparticles
FESEM	Field emission scanning electron microscope
FTIR	Fourier transform infrared
XRD	X-ray diffraction
EOR	Enhance oil recovery
EDS	Energy dispersive X-ray spectroscopy
DLS	Dynamic light scattering
IFT	Interfacial tension
PV	Pore volume

[1]Petroleum Engineering Department, Chemical Engineering Faculty, Tarbiat Modares University, Tehran, Iran. [2]Biotechnology Group, Chemical Engineering Faculty, Tarbiat Modares University, Tehran, Iran. [3]Environmental Research Institute, Tarbiat Modares University, Tehran, Iran. ✉email: ajafari@modares.ac.ir; manteghi@modares.ac.ir

PTCC	Persian type culture collection
ZP	Zeta potential
θ_i	Initial rock wettability
θ_o	Original rock wettability
θ_f	Final rock wettability

Synthesis of nanoparticles (NPs) through green synthesis is an environmentally friendly and sustainable approach compared to the conventional chemical synthesis method[1,2]. It involves the utilization of natural resources such as organic systems and ideal solvent systems to avoid the production of unwanted or harmful by-products[3]. Bacteria, fungi, algae, and plant extracts can be used as reducing agents in the green synthesis of metal nanoparticles[3,4]. The use of microorganisms and plants to synthesize nanoparticles is called biosynthesis[5,6]. The advantages of green synthesis of nanoparticles include lower cost, decreased pollution, and overall, improved environmental conditions[7]. The process of green synthesis of nanoparticles involves the bio-reduction of metal ions into their elemental form in the size range of nanoparticles[8]. Synthesis of nanomaterial through this approach is an environment-friendly method that proves to be just as efficient if not more compared to other conventional synthesis techniques[9,10]. Choosing which microorganisms to use in creating nanoparticles involves considering factors, like the type of metal ions utilized the preferred size and shape of the nanoparticles, and the intended purpose of these nanoparticles[11,12]. Because bacteria are able to produce nanoparticles of different sizes, shapes, and morphologies, they are commonly used in the synthesis of nanoparticles. The application of bacteria provides several benefits, such as easy handling of growing conditions, rapid multiplication, and profitability[13,14].

Zinc oxide (ZnO) nanoparticles rank as the most prevalent metal oxide following iron. They are cost-effective, safe, and simple to produce. These nanoparticles find utility, in sectors, like rubber manufacturing, pharmaceuticals, petroleum extraction, textiles, biosensors, cosmetics, and more. Biosynthesized ZnO nanoparticles exhibit enhanced surface characteristics compared to those synthesized chemically making them ideal, for applications like reducing tension, between oil and water[15,16]. Tripathi et al. reported that zinc oxide nanoparticles can be formed through enzymes secreted by *Bacillus licheniformis* bacteria cells. In their studies, they used zinc acetate as a precursor salt. Zinc acetate and sodium bicarbonate react and form $Zn(OH)_2$, which is thermally destroyed and forms ZnO nuclei. Then the enzymes produced by bacteria produce zinc oxide nanoparticles[17]. Selvarajaran et al. used the bacterium *Lactobacillus plantarum* and the zinc sulfate precursor salt to produce nanoparticles of zinc oxide. They succeeded in the biological production of nanoparticles with a size of 13 nm and a spherical shape. They stated that in addition to the enzyme produced by bacteria, electro-kinetic potential and pH play an important role in the production of nanoparticles[18]. Libin et al. investigated the biosynthesis of zinc oxide nanoparticles using *Tinospora cordifolia* stem extract. In their reports, they discussed the effect of green synthesis of nanoparticles in reducing environmental problems and introduced the production of nanoparticles from this method as very important and effective. The produced nanoparticles with an average size of 47 to 87 nm were identified in the FESEM test, and according to the EDS test, 60% of the produced nanoparticles were reported to be zinc. In their research, they also studied the significant effects of biologically synthesized zinc oxide nanoparticles, in their anti-fungal and anti-bacterial properties[19]. Shanmugam et al. investigated the synthesis of zinc oxide nanoparticles using probiotic bacteria (*Lactobacillus fermentum*) as the reducing and capping agent. AFM analysis revealed that the nanoparticles' size was about 90–100 nm. In their study, the maximum concentration, 20 m Molar of ZnO NPs, showed the highest antimicrobial activity. These observations indicate that the synthesized ZnO NPs possess remarkable antimicrobial potency[20]. Green nanocomposites based on eucalyptus and walnut shells significantly enhance oil recovery in carbonate reservoirs by improving wettability and interfacial tension reduction under varying saline conditions, offering a stable, and efficient alternative for EOR applications[21]. Oil and gas industries have found that nanoparticles are the most viable solution for Enhanced oil recovery due to their characteristics. Oil recovery rates have been improved through the use of various types of nanoparticles in the conducted studies. The utlized nanoparticles are oxides of metals, such as nickel oxide, Zinc oxide, Aluminium Oxide etc. Altering viscosity, density, interfacial tension and the wettability of the reservoir (generally from oil-wet to water-wet reservoir) are some of the nanoparticle oil recovery mechanisms[22–27]. Ahmadi et al., synthesized a novel ZnO–TiO_2/ZSM-5 nanocomposite (ZTZ) for EOR in sandstone formations. The ZTZ outperformed the standalone ZSM-5 by improving stability, wettability, and IFT at reservoir conditions. ZTZ optimized capillary force alteration, which promoted oil detachment and accelerated production. At an ideal concentration, ZTZ achieved 9% higher oil recovery than ZSM-5 alone, establishing its efficiency as an EOR agent in sandstone reservoirs[28]. Leshari et al. compared the effect of several nanoparticles on the Enhanced oil recovery in reservoirs. They stated that zinc oxide nanoparticles can reduce the interfacial tension by 3×10^{-5} N/cm and increase oil recovery by 8%. The analyzed oil sample was from the Tapis oil field in Malaysia[29]. Ahmadi et al. investigated the application of cerium-modified ZnO nanocomposites to enhance oil recovery in sandstone reservoirs. By modifying ZnO with cerium, the nanocomposites demonstrated increased pore volume, stability, improved IFT, and CA reduction. Optimal concentration testing (100 ppm) at reservoir conditions (60 °C and 1800 Psi) showed that ZnO-Ce nanocomposites significantly enhanced the recovery factor from 37.11% (for unmodified ZnO) to 71.40%[30]. Another study investigated activated carbon–ZnO nanocomposites (AC/ZnO) for EOR in sandstone reservoirs. At 80 °C and 2500 Psi, various concentrations (30 to 180 ppm) were tested for wettability alteration, interfacial tension, and zeta potential, and 90 ppm was found to be optimal for both AC/ZnO and pure ZnO. AC/ZnO demonstrated superior performance, reducing the contact angle from 56.27° to 39.14° and increasing ZP from −37.79 to −42.06 mV. In oil recovery tests after 15 days, recovery factors were 38.38% for the base case, 51.79% for ZnO, and 66.68% for AC/ZnO, highlighting AC/ZnO's effectiveness in improving oil recovery[31]. Soleimani et al. investigated the performance of zinc oxide nanoparticles in reducing the interfacial tension between water and oil,altering the wettability of the reservoir

rock, and finally enhancing the oil recovery. At 0.3 wt% of ZnO nanoparticles, the results reveal a maximum surface tension of 35.57 mN/m. It was discovered that the nanofluid with the highest surface tension (0.3 wt%) had a higher recovery efficiency. The reduction of oil/water interfacial tension and alteration of wettability is the main cause for the highest recovery factor of 11.82% at 0.3 wt%[32].

In the current study zinc oxide was employed to synthesize nanoparticles using *Enterobacter cloacae* (PTCC: 1798) microorganism as a novel approach. For this purpose, this microorganism was extracted from the formation water of an oil field in the southwest of Iran. Plus, characterization tests such as; FTIR, FESEM, XRD, EDS, and DLS were carried out in order to identify and validate the characteristics of the synthesized nanoparticles. In the next step, the effectiveness of the base fluids, namely deionized water, seawater, and twice diluted seawater was explored and the role of ions was assessed. Then, the stability of nanofluids was tested by zeta potential and UV-vis spectrophotometer to optimize the concentration of nanofluids in several ranges (100, 500, 1000, and 2000 ppm). After that, the efficiency of the prepared nanofluids in absorption and rock wettability alteration was evaluated by interfacial tension and contact angle tests. Eventually, the oil recovery factor analysis was investigated through displacement tests inside a transparent 2-D micromodel as a microscopic scale to understand mechanisms by flow patterns.

Materials and methods

Microorganism and its growth conditions

In selecting the type of bacteria, the most crucial characteristic that should be considered is its ability to produce nanoparticles and the investigation of its performance in enhanced oil recovery. As such, *Enterobacter cloacae* microorganism with the PTCC: 1798 was selected for this research. This microorganism was isolated from the formation water of an oil field in the southwest of Iran. Figure 1 shows the microscopic image of the isolated bacteria. The specific growth medium for the desired microorganism is comprised of peptone (Merck. CAS number: 91079–38 – 8), meat extract (Merck. CAS Number: 68990–09 – 0), and $MnSO_4$ H_2O salt (Merck. CAS number: 10034–96 – 5). In the growth medium, the bacteria were inseminated and then they were put in a shaker incubator (Wise, 20 R; Korea) at a temperature of 37 °C and the rotational speed of 135 rpm for 8 h.

Utilized fluids

The oil for research is supplied from one of the reservoirs (southwest of Iran), with a viscosity of 540 centipoise and an API of 22. Furthermore, the SARA test results of crude oil have been tabulated in Table 1.

Deionized water was used in the synthesis phase of nanoparticles. Deionized water and Persian Gulf seawater (Cl^-: 23000, SO_4^{2-}: 3350, HCO^{3-}: 166, Mg^{2+}: 2996, Ca^{2-}: 267, Na^+: 11750, K^+: 499, Fe^{2+}: 0.42, Sr^{2+}: 3.4, TDS: 40270 ppm) were used in the interfacial tension, contact angle, and flooding tests in the micromodel.

Green synthesis of zinc oxide nanoparticles and its identification tests

After the cultivation of the *Enterobacter cloacae* microorganism with the PTCC: 1798 and their complete growth inside the incubator, the solution is centrifuged, and the solid components are separated and washed four times using deionized water. After that, it is added to 100 cc of deionized water and placed on a magnetic stirrer. Then, 20 cc of zinc acetate precursor salt (Merck. CAS Number: 5970-45-6) solution with 0.5 molar concentration is placed in the incubator for 24 h. After 24 h, the solution is placed in a centrifuge for 10 min (8000 rpm) at 4 °C and washed multiple times with deionized water and ethanol. After the following steps, the substance is placed

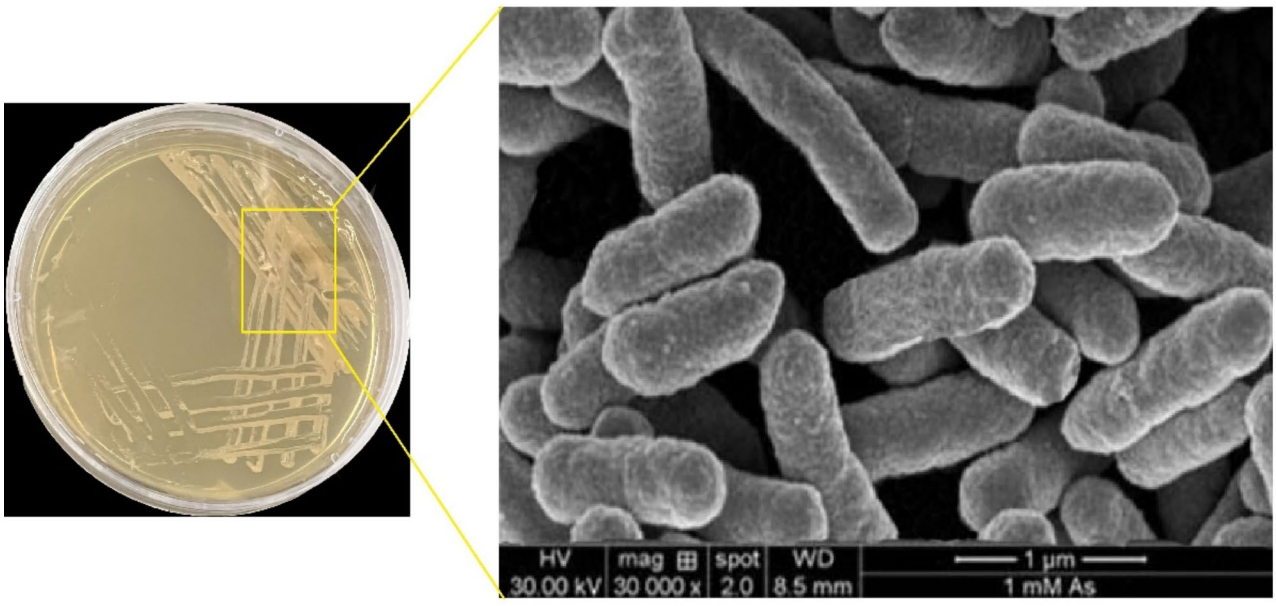

Fig. 1. Microscopic image of the isolated bacteria.

Properties	Count (Wt. %)
Saturate	34.41
Aromatics	41.94
Resin	6.45
Asphaltene	17.2

Table 1. Results of SARA analysis.

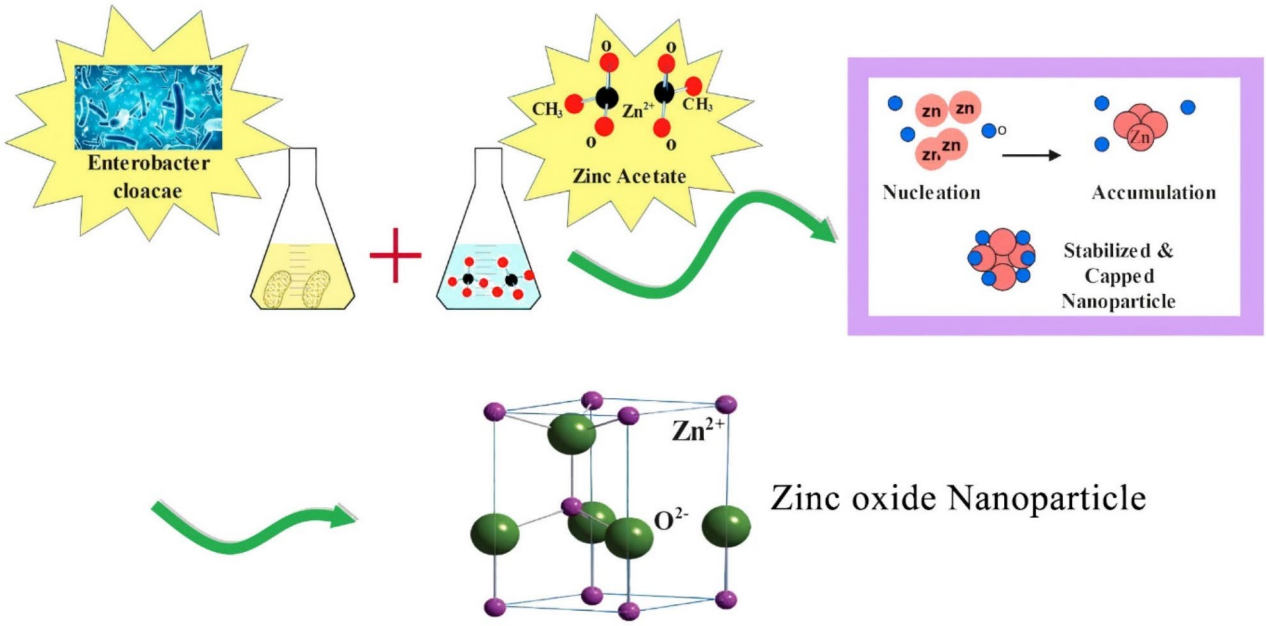

Fig. 2. Schematic of biosynthesis of zinc oxide nanoparticles.

in an oven (100 °C) for drying purposes. And finally, it is placed in a furnace/oven for 6 h at 400 °C with a 5 °C/min heat rate. Figure 2 shows the schematic of the biosynthesis of zinc oxide nanoparticles.

To verify the successful synthesis of the nanoparticles, various analytical methods were applied. X-ray diffraction (MPD XPert, Netherlands) and Fourier transform infrared spectroscopy (PerkinElmer-Frontier, USA) were used to assess the nanoparticles' composition. Field emission scanning electron microscopy (FEI NOVA NanoSEM 450, USA) characterized the size and morphology of the ZnO NPs, while dynamic light scattering (Nanotrac Wave-Microtrac, USA) measured particle size distribution in solution. Additionally, Energy Dispersive X-ray Spectroscopy (VEGA3, TESCAN, France) provided elemental and chemical analysis. Finally, the zeta potential test (Nanotrac Wave-Microtrac, USA) was carried out to stability assessment.

Measurement of interfacial tension

In this research, in order to measure the interfacial tension between oil and fluids, the Tensiometer device (KRUSS K11, Germany) and the ring method have been used. For this purpose, the ring was positioned just below the interface between the two immiscible liquids, then the ring slowly lifted through the interface using the tensiometer. As the ring moved upward, the lower-phase liquid adhered to it, creating a meniscus. Lifting until the force required to reach a maximum value was achieved, just before the liquid film broke. This peak force was recorded, and the tensiometer calculated the IFT, using a correction factor to account for the ring's dimensions. For accuracy, the measurement was repeated three times, and the mean value was reported.

Porous media

In order to apply reservoir conditions to the tests, a glass micromodel designed after a dolomite rock sample was used as the porous media. The schematics of the utilized micromodel are shown in Fig. 3. Table 2 shows the specifications of the micromodel.

The method for preparing and flooding the micromodel is as follows. Firstly, the micromodel is washed with water, toluene, and methanol. Afterward, it is dried using a vacuum pump and is soaked in a 0.5 molar sodium hydroxide solution for one hour so that it becomes oil-wet. Thereafter, the micromodel is washed with distilled water and dried in an oven at 200 C for 15 min, after which the micromodel is soaked in a 2% volume solution of

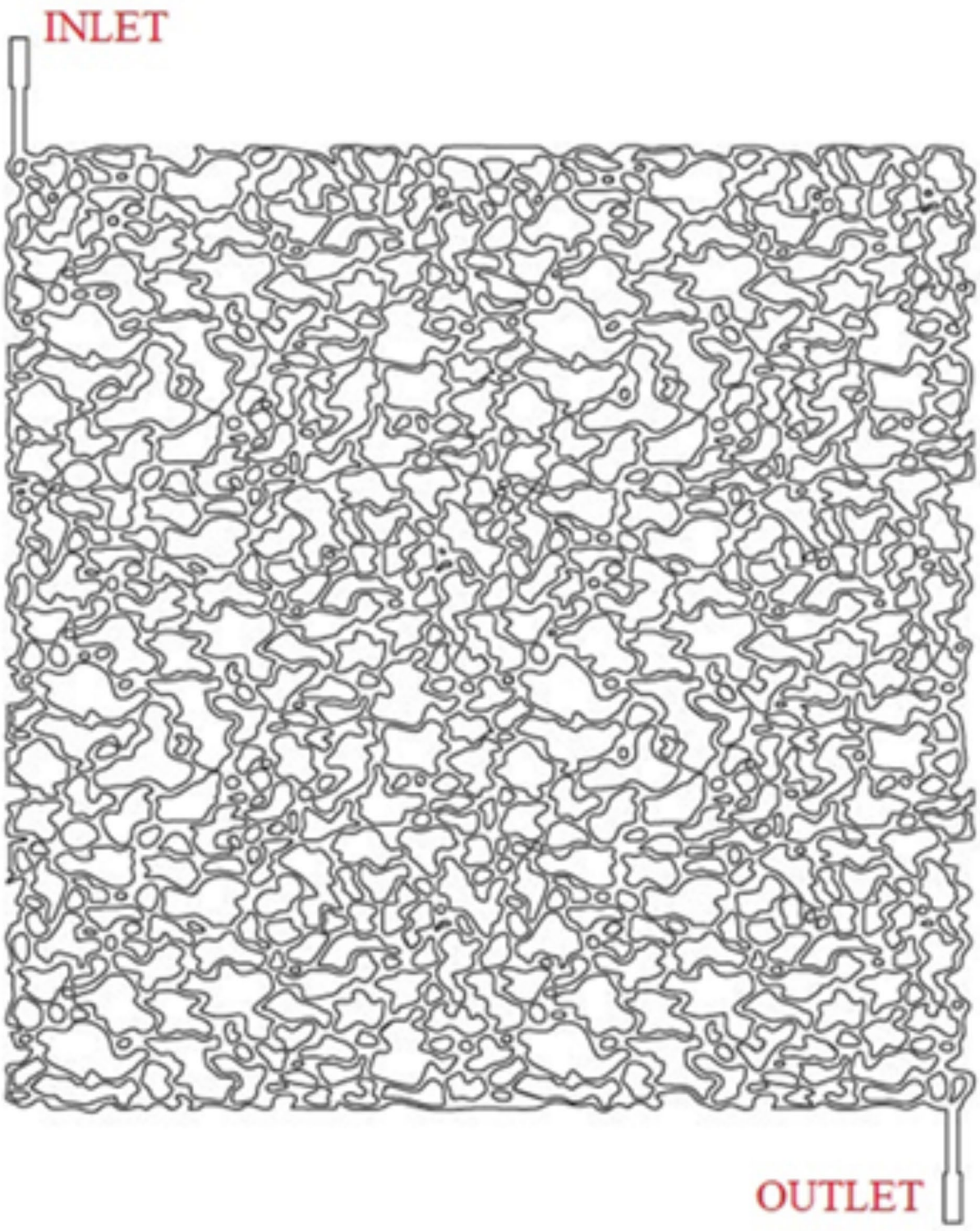

Fig. 3. Schematic of the dolomite micromodel.

Properties	Size (cm)	Thickness (μm)	Pore volume (cc)	Porosity (%)	Permeability (mD)
micro model	6×6	110	0.146	38	870

Table 2. Specification of the micromodel.

Trimethylchlorosilane for 5 min. After washing the micromodel with methanol to remove the excess silane, it is placed in an oven at 100 °C for an hour and vacuumed again. During the flooding operation, oil is injected into the micromodel at a rate of 0.07 ml/h. The solutions are injected into the porous media up to one pore volume. To calculate the recovery factor, the micromodel is photographed at one-minute intervals, and the amount of oil recovery is determined by analyzing these images.

Preparing thin sections of carbonate rocks for wettability experiments

Thin sections from carbonate rocks are prepared from the rock samples, with a thickness of 2 mm and a diameter of 1.5 in. To remove organic and inorganic materials from the rock surfaces.

The thin sections were washed with toluene, methanol, and formation water for 10, 3, and 2 days respectively. In the next step, the thin sections are placed in containers with the desired oil sample for 30 days at 75° C in an oven to become oil-wet and ready for the experiments.

Wettability alteration test

Wettability refers to the tendency of a liquid to contact a solid surface coated with another fluid (gas or liquid), which is mainly due to the existing intermolecular forces. The angle that a liquid droplet creates with a solid surface is called the contact angle, which is crucial in determining wettability. In this study, the sessile drop method was used to measure the contact angle. The schematic of the contact angle measurement device is shown in Fig. 4. Glass slides used in the micro-model construction were cut into smaller dimensions and grooves were made on them using a drill to resemble the porous media. In the next step, the glass slides were made oil-wet using the method mentioned in previous sections. To conduct the experiments, the glass slides were placed in the desired solutions for 4 h, and the contact angle of the oil was measured in each state. Each measurement was repeated three times, and their average was reported to minimize errors.

To measure the contact angle with the rock, the desired samples are prepared from the core using the method described above and made oil-wet before measuring the contact angle. Of course, before becoming oil-wet, the samples are made water-wet by being placed in formation water, and the contact angle is measured on these samples as the initial wettability of the rock (θ_i). After becoming oil-wet, the thin sections' contact angles are measured, and considered as the original wettability of the rock (θ_o). In the final step, after placing the rock samples in the desired nanofluid solutions, the contact angle is once again measured and considered as the final wettability of the rock (θ_f). Thereby, the wettability index is calculated using the following formula.

$$WA_{Index} = \frac{\theta_o - \theta_f}{\theta_o - \theta_i} \tag{1}$$

As the wettability index approaches one, it indicates a greater change in wettability, and as it approaches zero, it indicates no change in wettability.

Result and discussion

Identification of the biological nanoparticle

The results of the FTIR test for the produced nanoparticle from the precursor salt of zinc acetate are demonstrated in Fig. 5. The peaks at 1651 and 3304 correspond to the stretching and bending vibrations of the OH group and

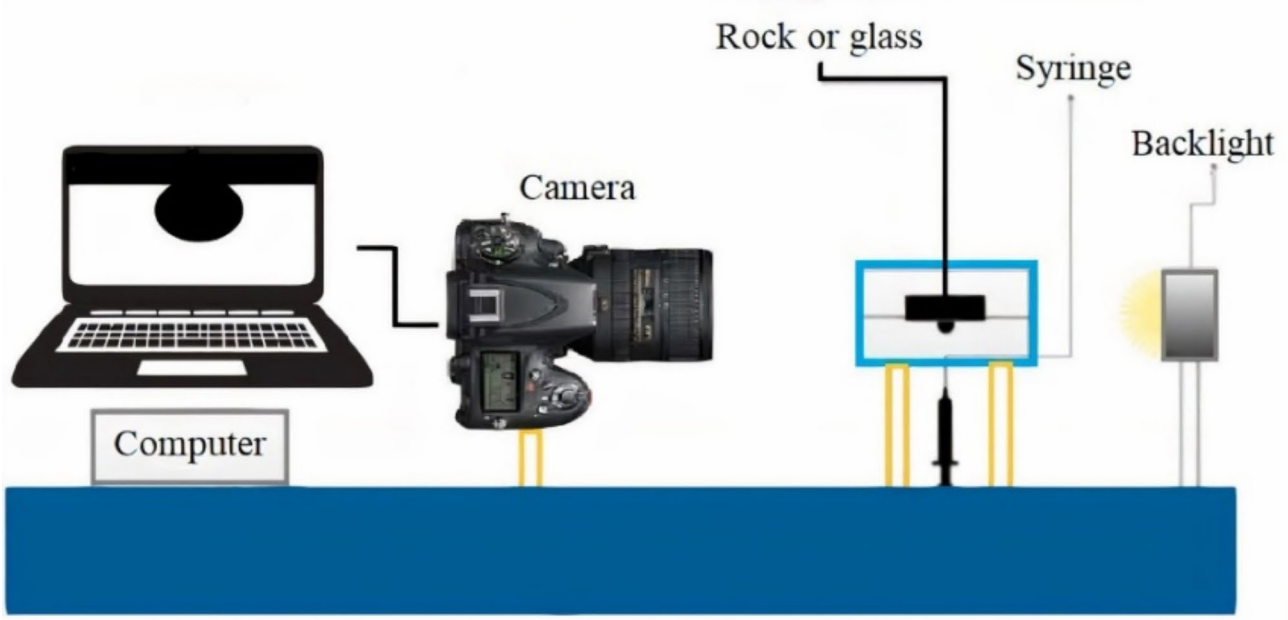

Fig. 4. Schematic of the Wettability alteration test's device.

can be indicative of the physical absorption of water on the surface of the nanoparticle. Furthermore, the peak at 2353 corresponds to the stretching bond of C=O and the peak at 1312 corresponds to the bending bond C–H which is abundant in precursor salt of zinc acetate. Lastly, the peak at 953 corresponds to Zn–OH, and the main peak at 463 corresponds to the Zn–O bond[33,34].

The XRD test results of the solid powder produced from the precursor salt of zinc acetate are illustrated in Fig. 6. As is shown, the peaks at the (2θ), 31, 36, 56, and 68 positions are indicative of zinc material presence[35,36]. The initial large peak indicates the amorphous nature of the product, which is due to the production of the intracellular nanoparticles underlying the bacterial biomass. As such, DLS, FESEM, and EDS tests are performed to identify the size of the produced biological Nano-particles and to analyze their elemental and imaging properties.

Figure 7a shows the DLS test results, applied to accurately measure the size of the nano-particles. This test is one of the most crucial tests for identifying the size distribution of nano-particles, revealing the hydrodynamic size of the particles. As is observed, most of the zinc oxide particles synthesized by the precursor salt of zinc acetate on the peak of 48 nm (the highest density in the range of 30 to 70 nm), and the polydispersity index, a parameter representing the size distribution of particles, is 0.342. The closer the value of the polydispersity index is to one, the size distribution of the particles is in a wider range. The produced zinc oxide nanoparticles are smaller than the pore size in the micromodel. Therefore, these particles will not block the flow path during the micromodel injection test. The elemental analysis results using EDS for the biological Nano-particle produced by the precursor salt of zinc and the percentages for each element are illustrated in Fig. 7b. The scarcity of the carbon elements, as portrayed in Fig. 7b, indicates that the precursor has thoroughly reacted with the solution obtained from the target bacteria, providing the conditions to produce Zinc oxide. The presence of a small amount of carbon is normal since the main substrate of the solution is organic and includes carbon-hydrogen and carbon-oxygen bonds. The weight percentages of zinc, oxygen, and carbon elements in the product are 51.52%, 36.04%, and 12.44%, respectively.

The FESEM test is implemented to examine the morphology of the particles present on the surface under investigation. Due to their small size, nanoparticles appear as a mass on the surface, and consequently, particle size obtained from FESEM is usually not accurate, and the displayed sizes are often exaggerated. Figure 8 shows FESEM images of biological zinc oxide nanoparticles produced by the acetate of zinc precursor salt. These images indicate the formation of nanoparticles in the range of 32–58 nm. Therefore, the size distribution of the synthesized nanoparticles in the FESEM test is in accordance with the results obtained from the DLS test and confirms this issue.

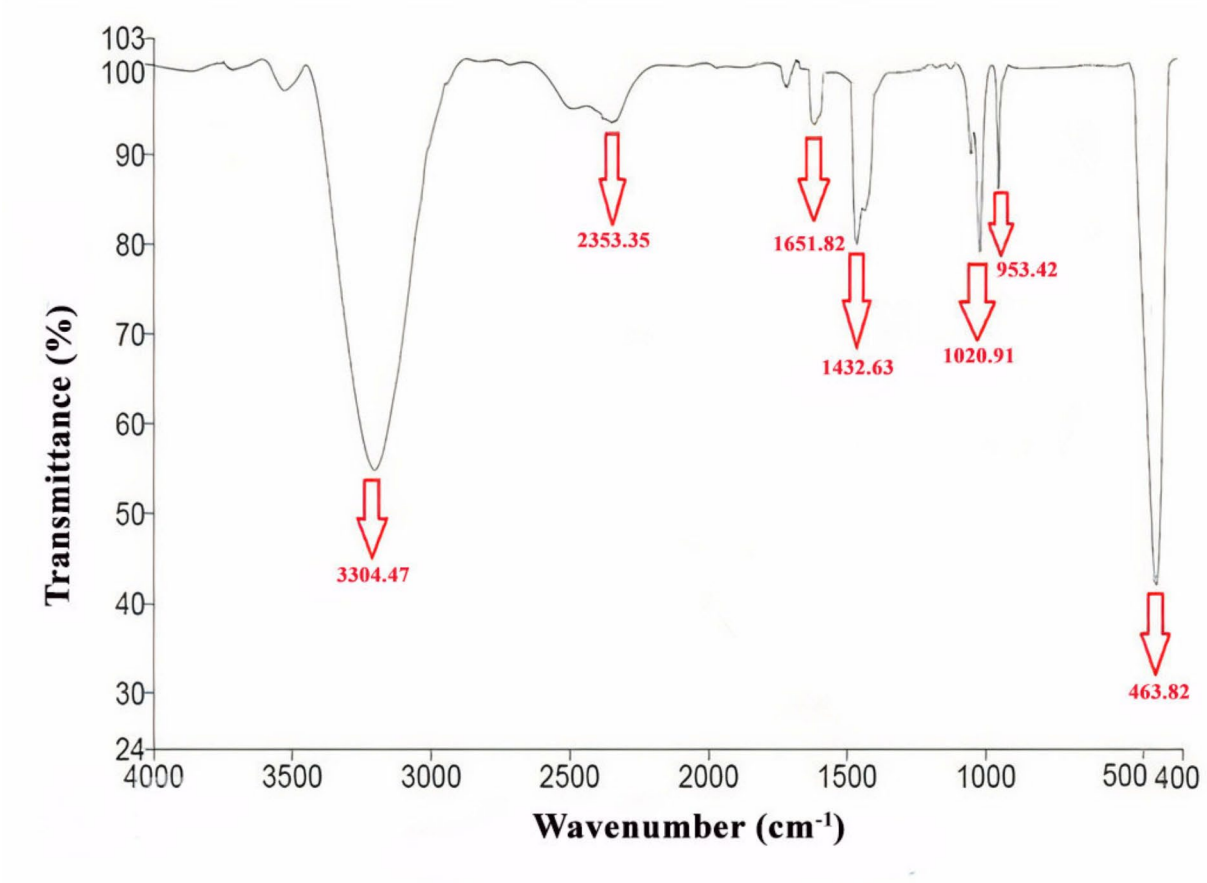

Fig. 5. FTIR spectrum for synthesized zinc oxide nanoparticle.

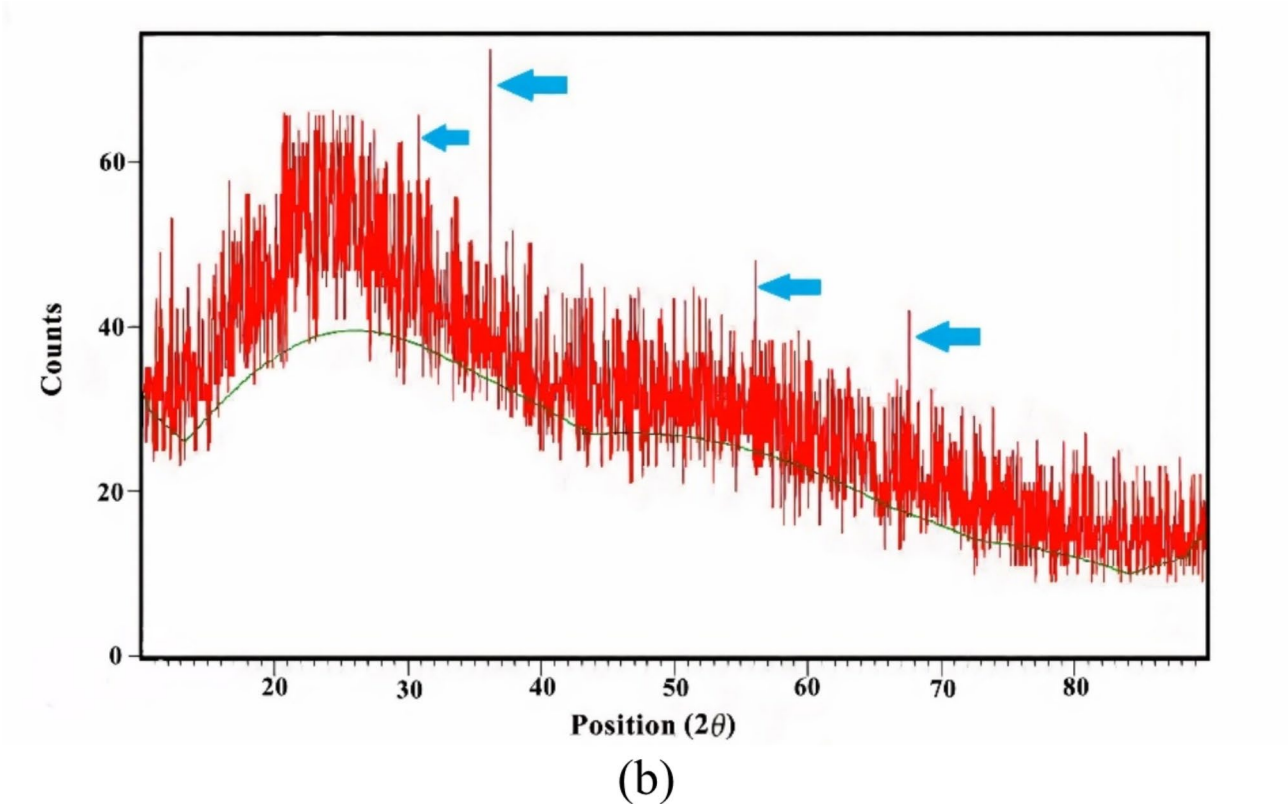

Fig. 6. XRD pattern for synthesized zinc oxide nanoparticle.

Investigation of the biological zinc oxide nanoparticle's stability

A high degree of stability for nano-fluids is required to inject them into the porous media without losing their properties. In this section, the stability of solutions containing biological zinc oxide nano-particles with concentrations of 100, 500, 1000, and 2000 ppm have been investigated. As shown in Fig. 9, produced zinc oxide nano-particles from the zinc acetate precursor salt have relatively good stability, and their precipitation occurs after 24 h at a concentration of 2000 ppm. However, at 100, 500, and 1000 ppm, the solution stability is maintained after 24 h, and no precipitation is observed. The instability of nano-fluids can lead to the accumulation of nanoparticles in the porous media and blockage of the existing flow paths, ultimately reducing the amount of oil recovery. Figure 13a quantitatively examines the stability of zinc oxide nanoparticles produced from the zinc acetate precursor salt. As shown in the graph, it is clear that the amount of light absorption remains almost constant at 100, 500, and 1000 ppm after 24 h, and no significant changes are observed. This indicates the stability of the nanofluid at these concentrations of biological zinc oxide nanoparticles. Plus, the zeta potential (ZP) experiment also demonstrated this result. The nanofluid indicated −36 mV ZP during the experiment (Fig. 10). This range of results illustrates that the prepared nanofluid has good stability, displaying no sedimentation of the nanoparticles and suggesting the prepared nanofluid is a good candidate for EOR applications in the long term[37]. However, the amount of light absorption decreases at 2000 ppm after 12 h, indicating instability and precipitation of the nanofluid.

Investigation of the effect of ions concentration in the base fluid on the stability of biological zinc oxide nanoparticles

One of the most critical parameters affecting the stability of nanofluids is the amount and concentration of salt ions in the base fluid. To investigate this parameter, Nanofluids at 100, 500, 1000, and 2000 ppm of biological zinc oxide nanoparticle concentrations were prepared in seawater and twice diluted seawater, and their stability was qualitatively and quantitatively examined. As illustrated in Fig. 11, the stability of nanoparticles over time at various intervals (12 and 24 h) was observed. This time evaluation is essential for understanding the flocculation and sedimentation. The observed stability across both time points at all concentrations, followed by sedimentation at higher concentrations (1000 and 2000 ppm), recommends an operation of time-dependent destabilization. This effect can be attributed to van der Waals attractions, which act at short distances and tend to draw particles together[38]. As the nanoparticle concentration upgraded, particles got closer to each other, thereby raising the attractive forces that overcome their interactions. A net attractive force that causes clump and sedimentation is the reason for balance shifts in concentrations above 1000 ppm.

Additionally, Fig. 12 shows the stability of biological zinc oxide nanoparticles in seawater that is diluted twice. As is observed, the nanofluid is stable in all of the mentioned concentrations after 12 h, and no precipitations are observed.

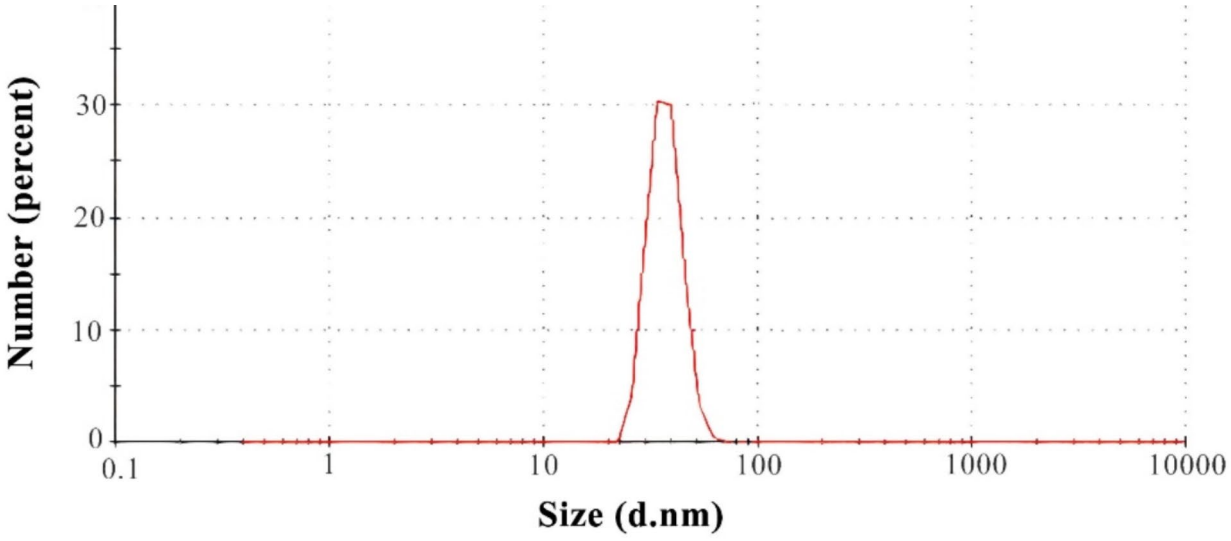

(a)

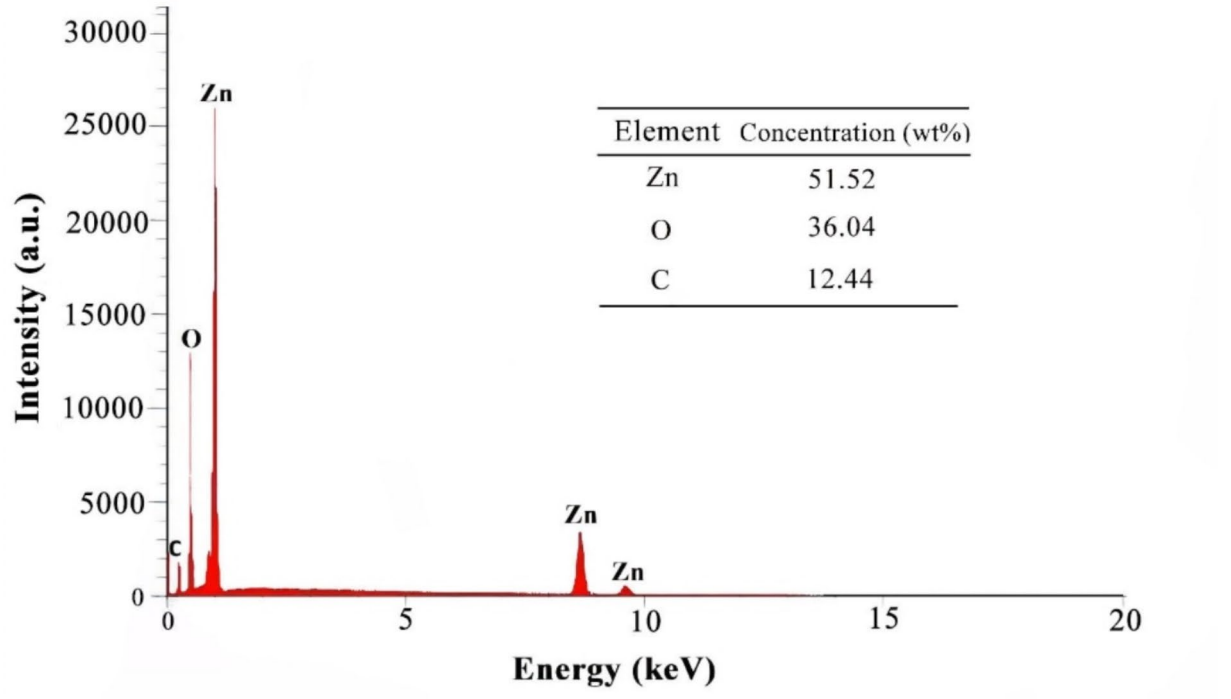

Element	Concentration (wt%)
Zn	51.52
O	36.04
C	12.44

(b)

Fig. 7. Synthesized zinc oxide nanoparticle, (**a**) DLS analysis. (**b**) EDS spectra.

After 24 h, samples with concentrations of 1000 and 2000 ppm exhibit partial precipitation due to the increasing particle-particle interactions over time. Consequently, van der Waals forces play a more prominent role in this setting. As particles draw closer to each other over time, these attractive forces can overpower the weakened electrostatic repulsion, resulting in a net attraction that boosts aggregation.

Figure 13b, c show a quantitative examination of the stability of zinc oxide nanoparticles at different concentrations in twice diluted seawater and seawater. In the UV-Vis spectrophotometer, UV light passes through the nanofluid dispersion, and the light intensity decreases exponentially as the nanofluid concentration

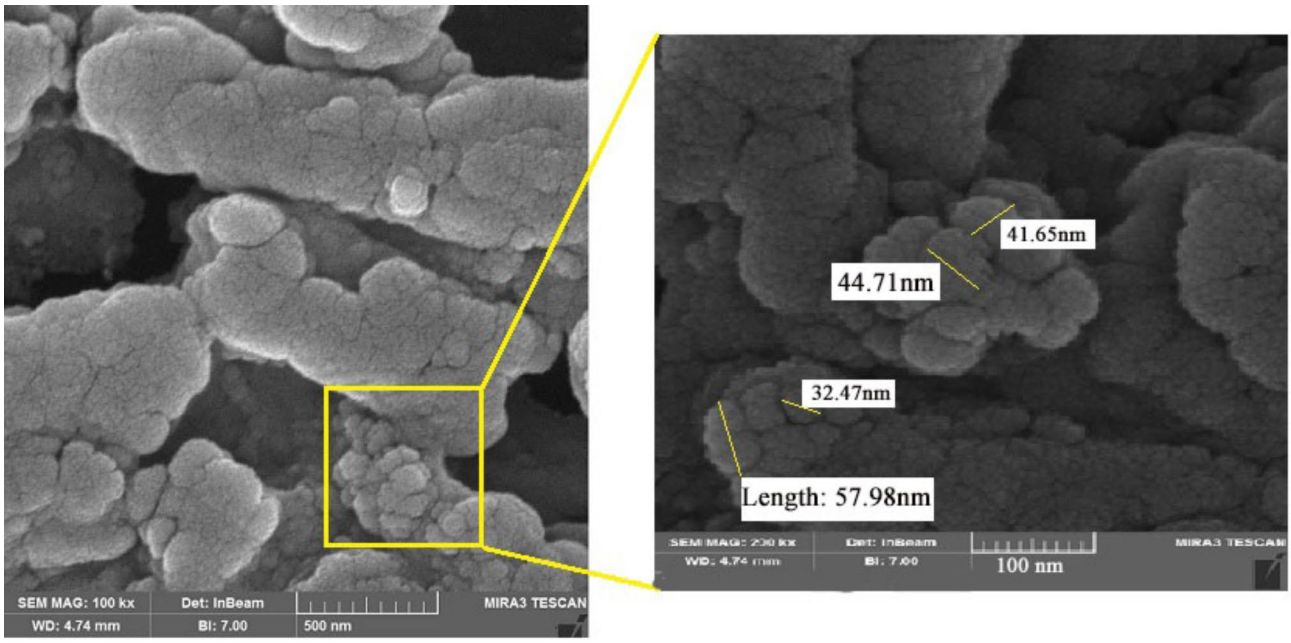

Fig. 8. FESEM image for synthesized zinc oxide nanoparticle.

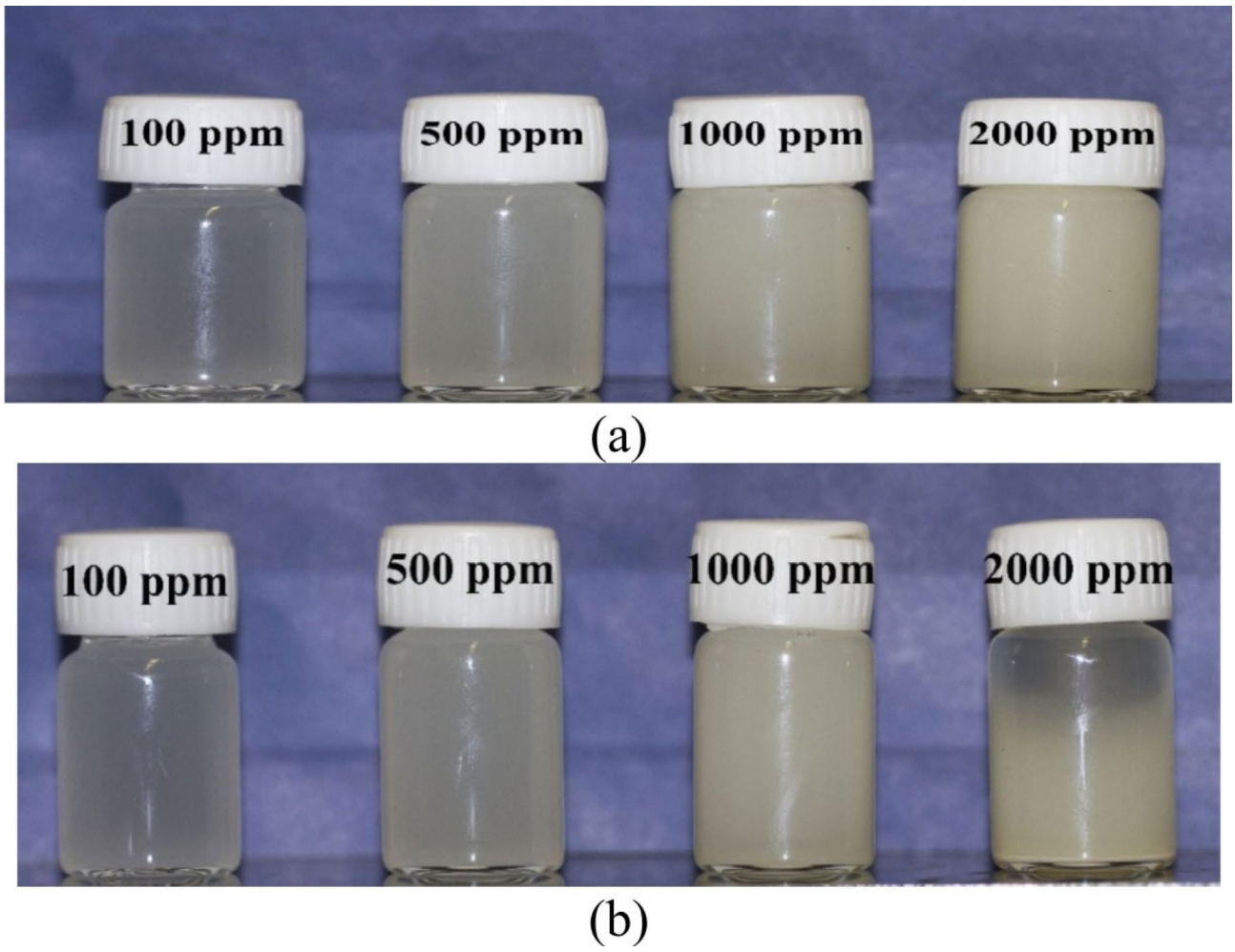

Fig. 9. Stability of synthesized zinc oxide nanoparticle in water (**a**) After 12 h, (**b**) After 24 h.

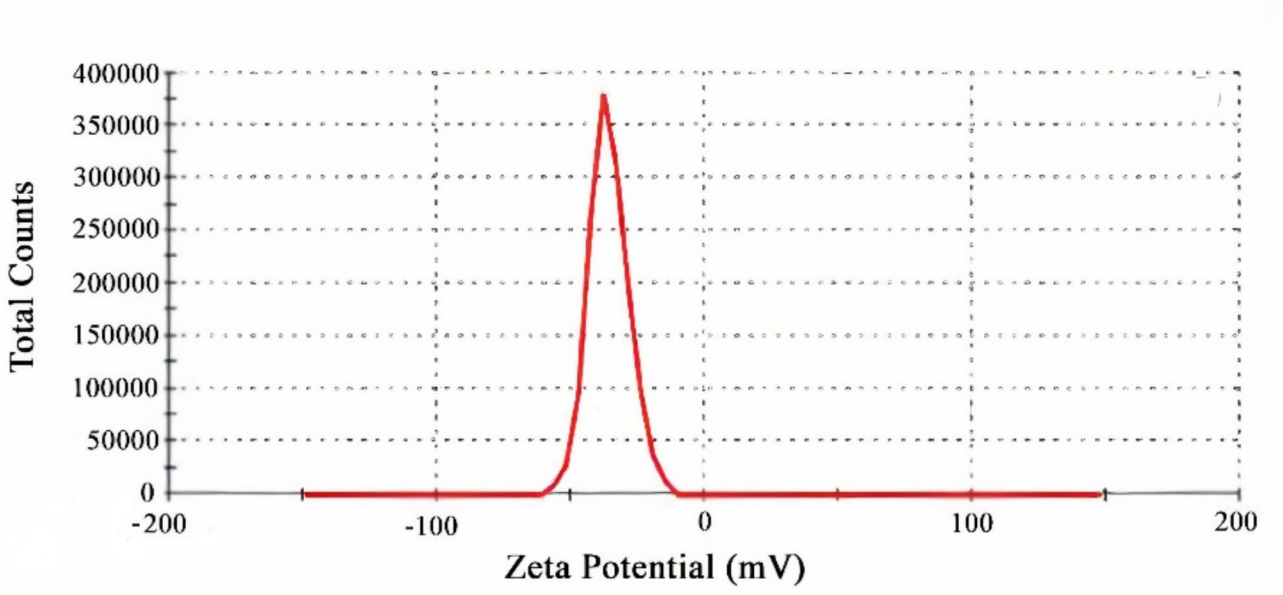

Fig. 10. Zeta potential of synthesized ZnO nanoparticle.

increases. In better words, as the concentration of nanoparticles decreases, the nanofluid becomes more transparent, leading to an increase in light transmission intensity and a corresponding decrease in absorption.

Interfacial tension test

One of the most crucial and influential parameters in the enhanced oil recovery process is the value of the interfacial tension between the injected fluid and the reservoir oil. The interfacial tension between the oil and the zinc oxide nanoparticle was measured at 100, 500, 1000, and 2000 ppm concentrations. As discussed earlier, the utilized base fluids were distilled water, seawater, and twice diluted seawater. Table 3 demonstrates the exact values of various fluids with oil in different concentrations of biological zinc oxide. The values in the table demonstrate that the biological nanoparticle causes a reduction of IFT. The main contributing factor to this is the higher surface charge leading to a higher surface activity which enables the formation of more bonds in the surface of water and oil. Consequently, when the biological nanoparticle is located in the oil-water interface, the contact surface is reduced considerably, leading to the reduction of the IFT.

The solubility of organic materials, such as asphaltene and resin are considerably higher In solutions with low salinity in comparison with solutions with high salinity. Consequently, in low salinity solutions, organic components with pseudo-surfactant attributes, actually act as a surfactant between the surfaces of water and the oil. As such they act accordingly and lower the interfacial tension more efficiently compared to high-salinity water dubbed as the salting in phenomenon. As the salinity and ion count increases in the water, the mobility of the salt ions towards the water phase increases. Consequently, the salt-water bonds will break on the surface. The presence of more ions in the water will eventually prevent asphaltene and resin from moving toward the water phase, leading to the surface concentrations of asphaltene and resin reaching negative values. Consequently, the interfacial tensions increase with salinity, dubbed the salting out phenomenon. Also, in isothermal conditions, the molecular movement in high-salinity water, is significantly lower compared to low-salinity water. Consequently, the oil-water interface has a thicker film, which within itself increases the interfacial tension.

Wettability alteration test

Wettability alterations (from oil-wet to water-wet) in reservoirs are one of the most important mechanisms for EOR. The surface of carbonate rock has a positive charge. However, when in contact with oil, heavy acidic components of the oil such as carboxylic acids with a negative charge are adsorbed on the surface of the carbonate rock with a positive charge, resulting in the surface becoming oil-wet. As various fluids such as seawater come into contact with carbonate rock, they change the wettability of the carbonate rocks to water-wet due to the presence of potential determining ions (Ca^{2+}, Mg^{2+}, and SO_4^{2-}). In other words, when such fluids come into contact with the carbonate rock surface, the SO_4^{2-} ion with a negative charge is adsorbed onto the carbonate rock surface (with a positive charge), weakening or eliminating the electric field of the carbonate rock surface, which in turn weakens the holding force of heavy polar compounds of oil on the rock surface (carboxylic acids with a negative charge). Similarly, cations such as Mg^{2+} and Ca^{2+} cause the separation of negatively charged carboxylic acid groups of crude oil from the rock surface by forming bonds with them when they come into contact with the reservoir rock. To conduct wettability tests, thin sections of carbonate rock were prepared and made oil-wet. Before the wettability test, the θ_i factor was measured and found to be 28° for the carbonate rock. After the test, the θ_o factor was measured and found to be 155°. In the next step, the thin sections were placed in nanofluids containing 500 and 1000 ppm of zinc oxide nanoparticles for a duration of three days. Finally, the θ_f factor was

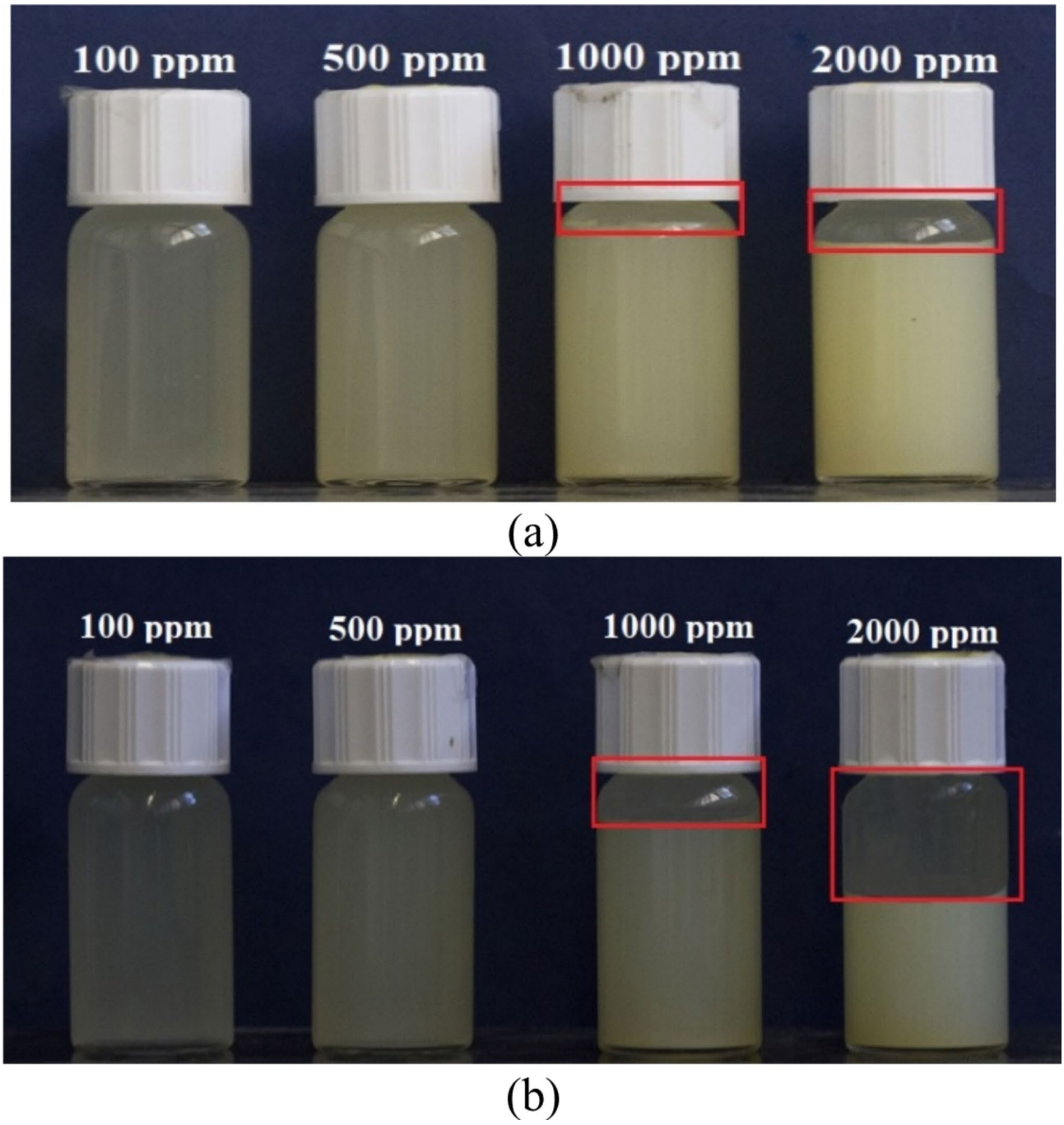

Fig. 11. Stability of synthesized zinc oxide nanoparticle in seawater (**a**) After 12 h, (**b**) After 24 h.

measured for each separate state, and the results are presented in Table 4. The contact angle of the oil droplet on the surface of distilled water was 140°, while on the surface of the twice-diluted seawater, it was 114°, and on the surface of seawater, it was 125°. The greater reduction in the twice-diluted seawater can be attributed to the presence of effective ions at their optimal surface concentration.

In the presence of nanoparticles, the hydrogen bond between water and the surface of the zinc oxide nanoparticle increases the surface energy, resulting in an increased surface tension between the liquid and solid, a decreased contact angle, and a more hydrophilic surface. Furthermore, an increase in the concentration of the nanoparticle fluid leads to an increase in the number of hydrogen bonds, creating more opportunities for adsorption onto the surface, and further decreasing the contact angle. Figure 14 shows the wettability index for nanoparticle-containing nanofluids and commercial zinc oxide at different concentrations and base fluids. Figure 15 shows the contact angle in carbonate rock in different states.

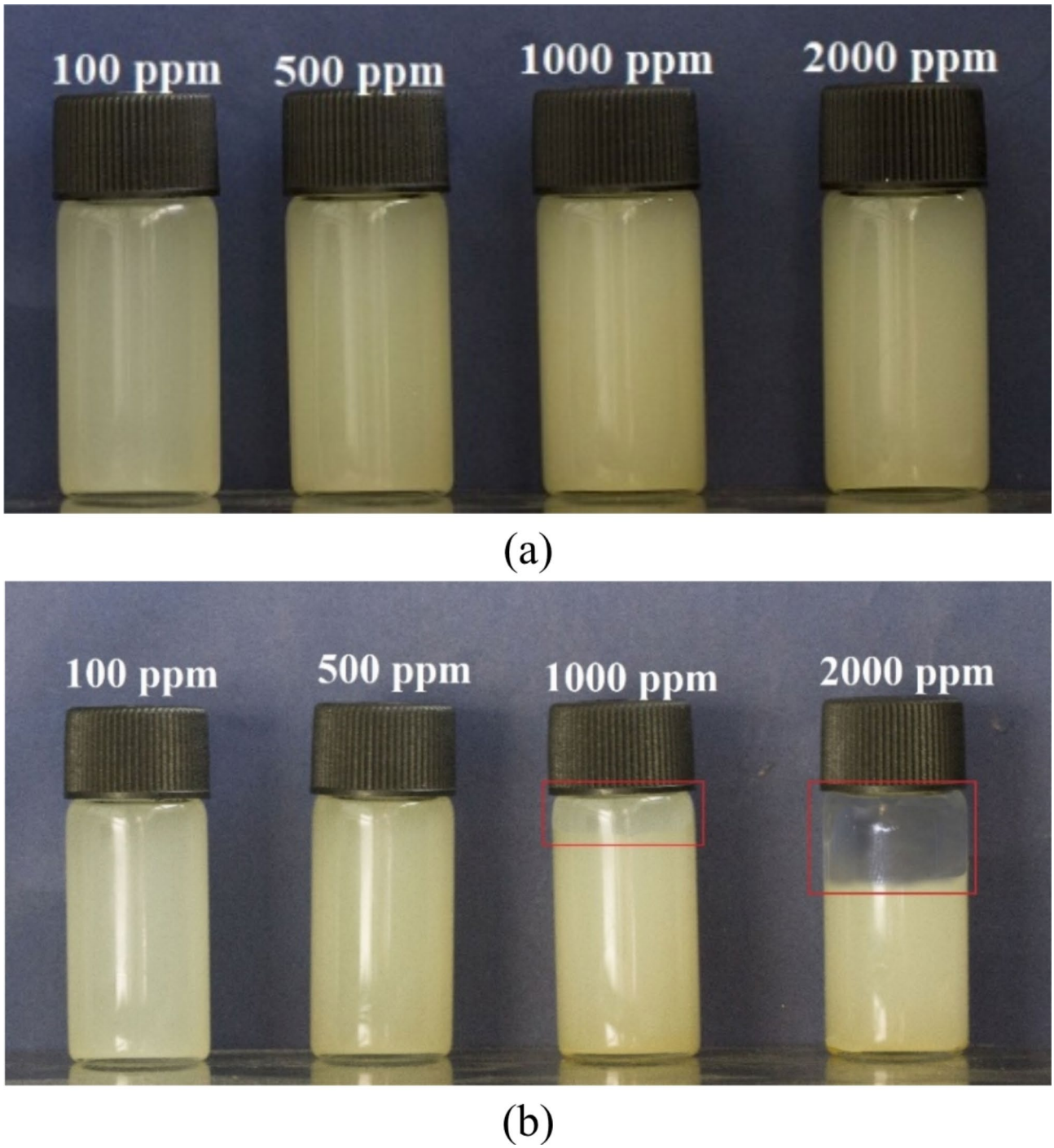

Fig. 12. Stability of synthesized zinc oxide nanoparticle in twice diluted seawater (**a**) After 12 h, (**b**) After 24 h.

Investigating the injection of fluids that contain biological ZnO nanoparticles into the micromodel

Deionized water as a base fluid

Initially, deionized water was injected into the micromodel to investigate its effect on enhancing oil recovery. As shown in Fig. 16a, the mobility ratio of injected fluid is unfavorable, and for this reason, due to the fingering phenomenon, water tends to pass through the most permeable and shortest possible path and reach the outlet of the micromodel. The low recovery of oil from water injection is a result of this phenomenon. The amount of oil recovered in this case is 20%. It is important to note that to ensure the reliability of the results, all the tests were repeated twice, and according to the small size of the error bar, the results of all the micromodel flooding tests have been reported as their mean. Figure 16b illustrates the injection of deionized water fluid that contains zinc oxide biological nanoparticles with a concentration of 500 ppm. According to the figure, the amount of oil

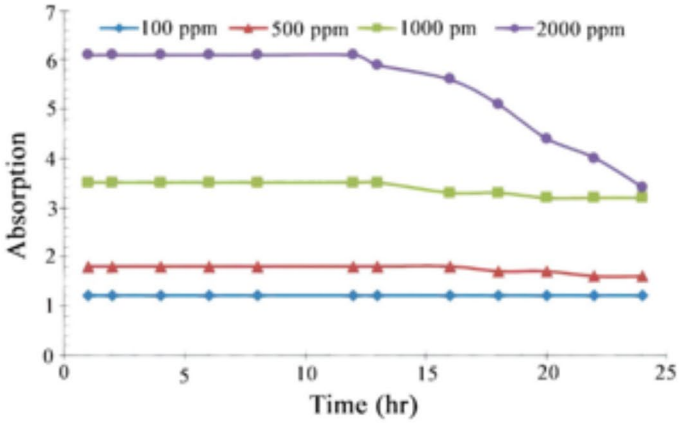

(a)

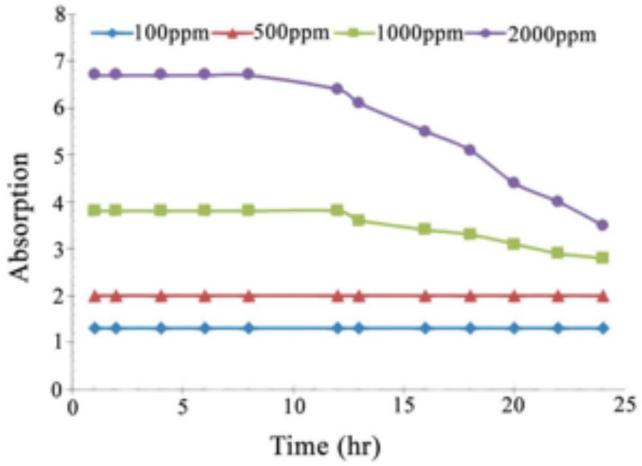

(b)

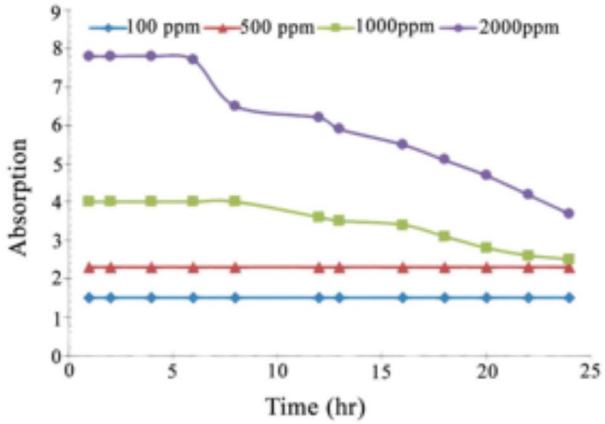

(c)

Fig. 13. Quantitatively examine the stability of synthesized zinc oxide nanoparticle in, (**a**) water, (**b**) twice diluted seawater, (**c**) seawater.

recovered in this case is 36%, 16% higher compared to the injection of deionized water without bio-nanoparticles. This increase is due to the effect of the nanoparticles and the reduction of interfacial tension between water and oil, as well as the lower mobility ratio of the injected fluid. Next, in order to investigate the effect of nanoparticle concentration on increasing oil recovery, a base fluid containing nanoparticles with a concentration of 1000 ppm was injected into the micromodel that was saturated with oil. The recovery rate for oil in this case has increased, as demonstrated in Fig. 16c, compared to the previous two injections. This case has a 43% recovery rate for oil.

Base fluid	NPs conc. (ppm)	IFT (mN/m)
Deionized water	0	28 ± 0.3
	100	21 ± 0.5
	500	17 ± 0.1
	1000	13 ± 0.1
	2000	11 ± 0.9
Twice diluted seawater	0	32 ± 0.3
	100	28 ± 0.3
	500	23 ± 0.5
	1000	19 ± 0.1
	2000	17 ± 0.1
Seawater	0	40 ± 0.5
	100	35 ± 0.2
	500	30 ± 0.9
	1000	27 ± 0.4
	2000	25 ± 0.2

Table 3. Interfacial tension test results.

Base fluid	NPs conc. (ppm)	θ_o	θ_i	θ_f	Type of wettability
Deionized water	0	155	28	140	Strongly oil-wet
	500	155	28	70	Water-wet
	1000	155	28	55	Water-wet
Seawater	0	155	28	125	Strongly oil-wet
	500	155	28	55	Water-wet
	1000	155	28	48	Water-wet
Twice diluted seawater	0	155	28	114	Strongly oil-wet
	500	155	28	45	Water-wet
	1000	155	28	39	Water-wet

Table 4. Contact angles of biological zinc oxide nanofluids on thin sections of carbonate rock (error bars were not added as they are small in size).

By injecting Nanofluid at a concentration of 1000 ppm, the efficiency of the porous bed sweeper is increased and the injected fluid is in contact with a larger volume of oil. This increase in the oil recovery rate is reasonable when considering the interfacial tension and wettability index in this and previous states.

Sea water as a base fluid

One of the parameters affecting the performance of biological nanoparticles is the type of base fluid. The presence of different ions in the fluid can result in different performances in oil recovery from reservoirs. Due to the presence of effective ions in seawater injection, it has a higher oil recovery rate compared to deionized water injection and establishes the electrostatic bond between ions and fatty acids with a negative charge in the oil. Figure 17a shows that the recovery rate of oil in this case is 26%, which has increased by 6% compared to deionized water. Figure 17b, c respectively show the injection of fluid containing biological nanoparticles with concentrations of 500 and 1000 ppm along with seawater base fluid, the oil recovery rate is 41% and 49%, respectively. The interfacial tension between the injection fluid and oil is reduced by the presence of biological nanoparticles. Furthermore, the 8% increase in the recovery is attributed to the higher wettability index at 1000 ppm compared to 500 ppm. Figure 17c indicates that the injection fluid front has moved completely uniformly and the fingering phenomenon has been greatly reduced compared to all the mentioned cases.

Diluted seawater as a base fluid

The performance of the diluted seawater fluid in enhanced oil recovery is shown in Fig. 18a. As illustrated in the figure, it outperforms the deionized water and the seawater as a base fluid. The oil recovery rate is 30%, and this increase of 10% and 4% is caused by the presence of positively charged ions such as calcium and magnesium at their optimum level. Also, the positive charge and the high ionic activity can lead to ions entering the stern layer and by forming a complex with negatively charged oil acid groups, which then causes these groups to accumulate on the contact surface, reducing the interfacial tension and improving oil recovery.

Figure 18b, c show the injection of bio-nanoparticles with concentrations of 500 and 1000 ppm along with the diluted seawater base fluid. The percentage of oil recovery in these cases is 50 and 56, respectively. The injection fluid front has moved uniformly, as demonstrated in Fig. 18c, and the efficiency of the porous bed

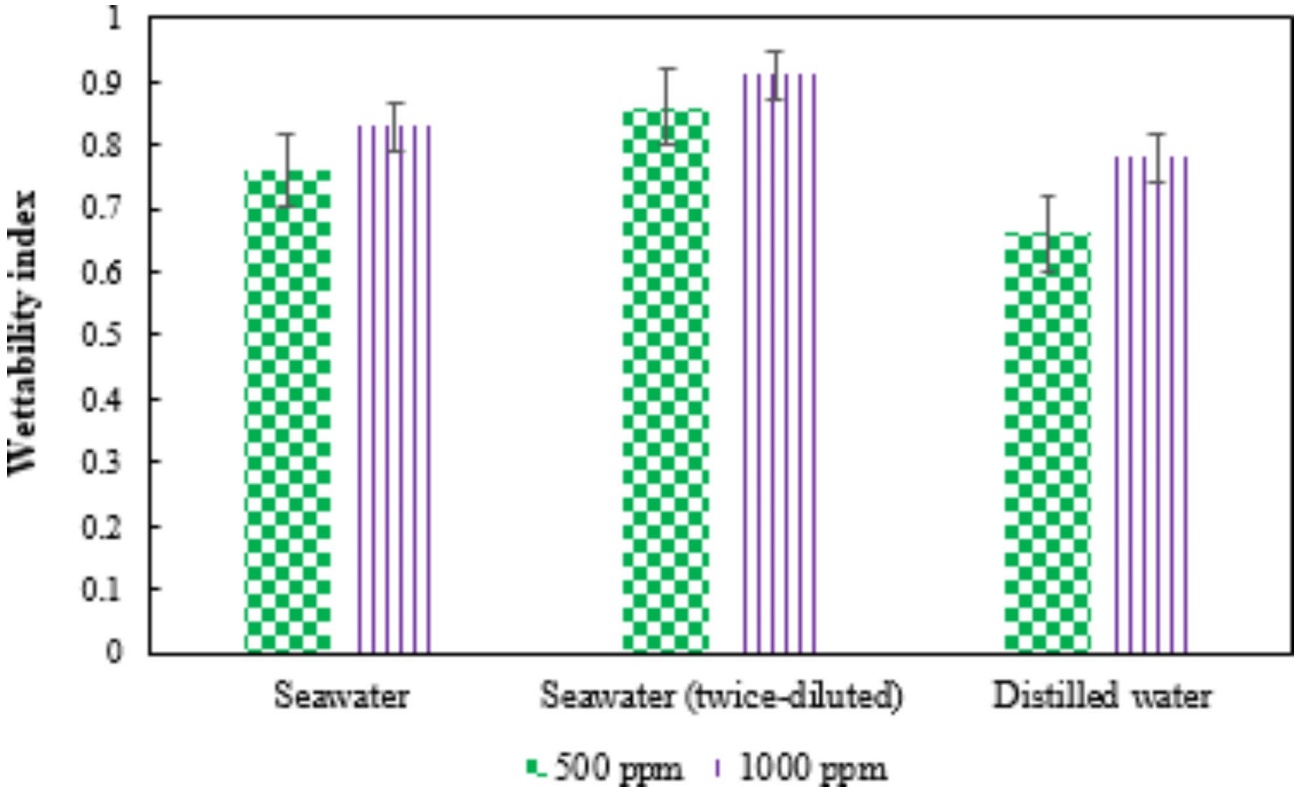

Fig. 14. Wettability index of the biological zinc oxide nanofluids on thin sections of carbonate rock.

sweep has greatly improved compared to injection in all the cases mentioned. Moreover, the effect of the change in wettability is one of the influential factors in this case, which has the highest wettability index relative to all cases. As such, it can separate the remaining oil from the porous bed wall and increase oil recovery by changing wettability to water-wet. Also, in fluids with low salinity, lowering the concentration of inactive salt, NaCl, has a positive effect on Enhanced oil recovery.

Conclusion

In this study, *Enterobacter cloacae* (PTCC: 1798) has been utilized in the biological synthesis of zinc oxide nanoparticles. Furthermore, the performance of the synthesized nanoparticle in enhanced oil recovery has been investigated. Several analytical methods FTIR, FSEM, XRD, DLS, and EDS, were used to analyze the produced ZnO NPs. According to the FTIR test, the 953 peak corresponds to the Zn–OH bond, and the main peak in the results at 463, corresponds to the Zn–O bond. The FESEM analysis confirmed the amorphous form and estimated NPs size in the range of 32 to 58 nm. In investigating the effect of synthesized nanoparticles in interfacial tension and stability tests, three base fluids (distilled water, seawater, and diluted seawater) and 5 levels of nanoparticle concentration (0, 100, 500, 1000 and 2000 ppm) were considered. The Full assessment of the IFT results concludes that with the increase of nanoparticle concentration up to 2000 ppm, the interfacial tension between oil and nanofluid decreases due to the placement of nanoparticles in the interface between the two fluids. Furthermore, the stability test results point out the fact that the concentrations of 500 and 1000 ppm of the produced biological nanoparticles are the most suitable options to investigate the wettability alteration and injection in the porous medium. According to the wettability test, zinc oxide biological nanoparticles can reduce the contact angle between oil and the porous medium from 155 degrees to 45 degrees, indicating the change of wettability of the porous medium from oil-wet to water-wet. The largest contact angle reduction is caused by the nanofluid with a concentration of 1000 ppm with the diluted seawater as base fluid, reducing the angle between the oil droplet and the porous medium by 116 degrees (down to 39 degrees). In this case, the wettability index is 0.91. In the investigation of the synthesized biological nanoparticles' effect on EOR, nanofluids with different base fluids (water, seawater, diluted seawater) were injected into the porous medium saturated with oil, in which the nanofluids with a concentration of 1000 ppm yielded the best results in terms of enhanced recovery. The highest oil recovery coefficient was 56% for the injection of nanofluid with a concentration of 1000ppm with the diluted seawater base fluid. In the injection of nanofluids with the base fluid of water and seawater with the same concentration of zinc oxide biological nanoparticles, the oil recovery rate was 43% and 49%, respectively. The main mechanism of increasing oil recovery was reducing the interfacial tension between oil and injected nanofluid, as well as changing the wettability of the porous medium from oil-wet to water-wet.

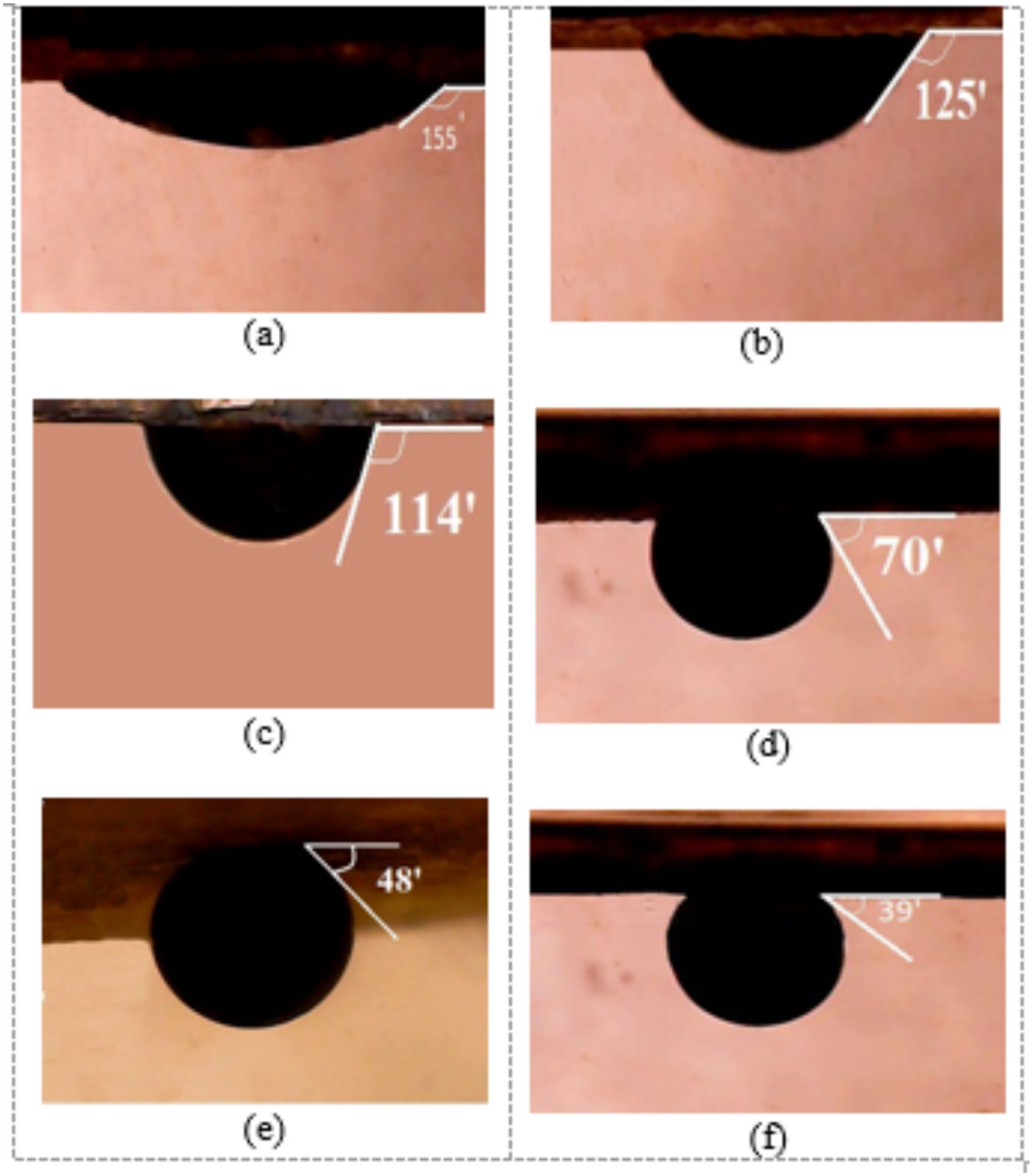

Fig. 15. The results of wetting the thin sections in (**a**) oil, (**b**) Sea water, (**c**) Twice diluted seawater, (**d**) Deionized water & ZnO (500 ppm), (**e**) Sea water & ZnO (1000 ppm), (**d**) Twice diluted seawater & ZnO (1000 ppm).

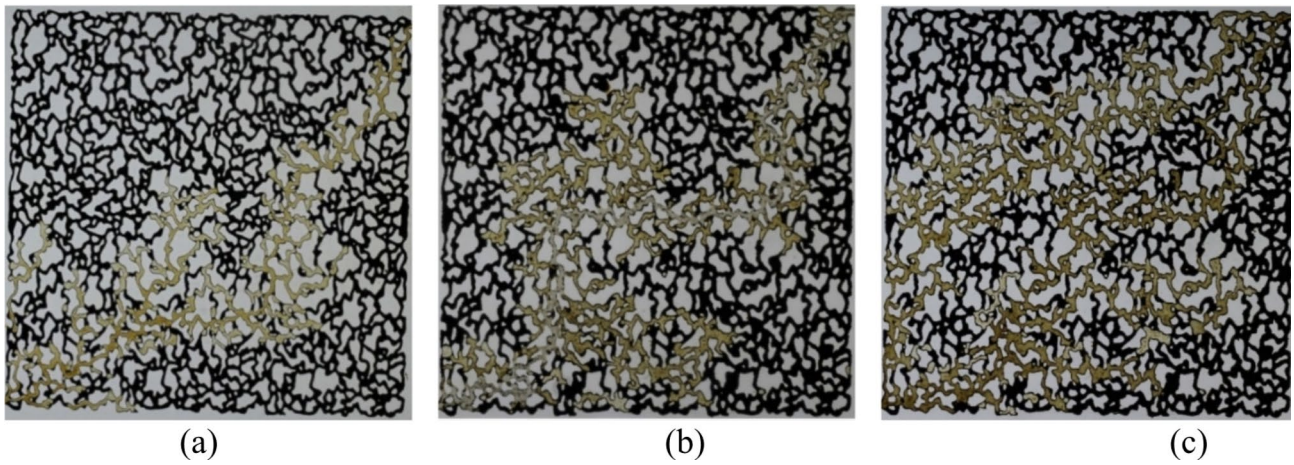

Fig. 16. Oil displacement during deionized water injection with biological zinc oxide NPs, (**a**) 0 ppm, (**b**) 500 ppm, (**c**) 1000 ppm.

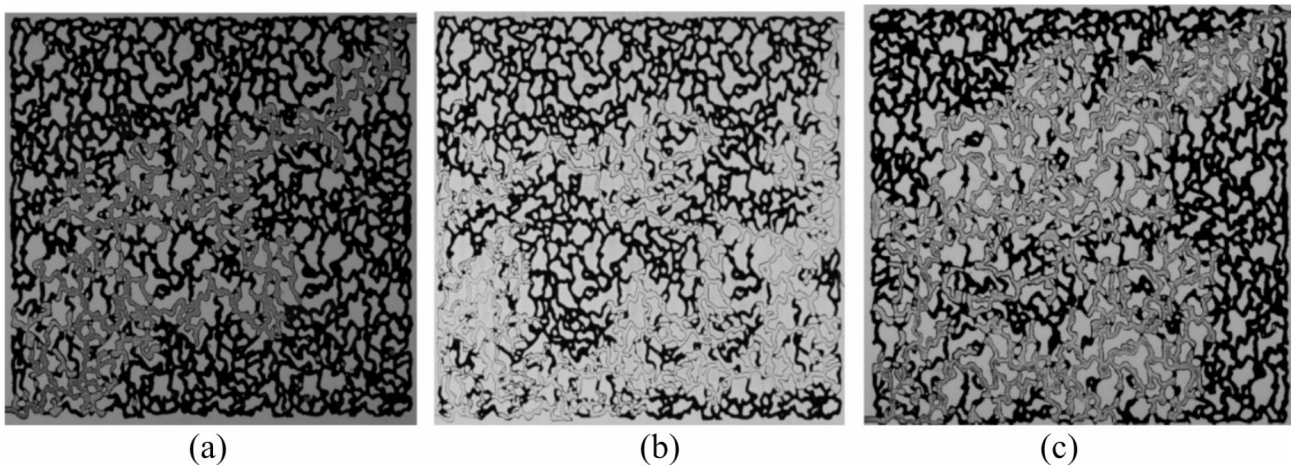

Fig. 17. Oil displacement during seawater injection with biological zinc oxide NPs, (**a**) 0 ppm, (**b**) 500, (**c**) 1000 ppm.

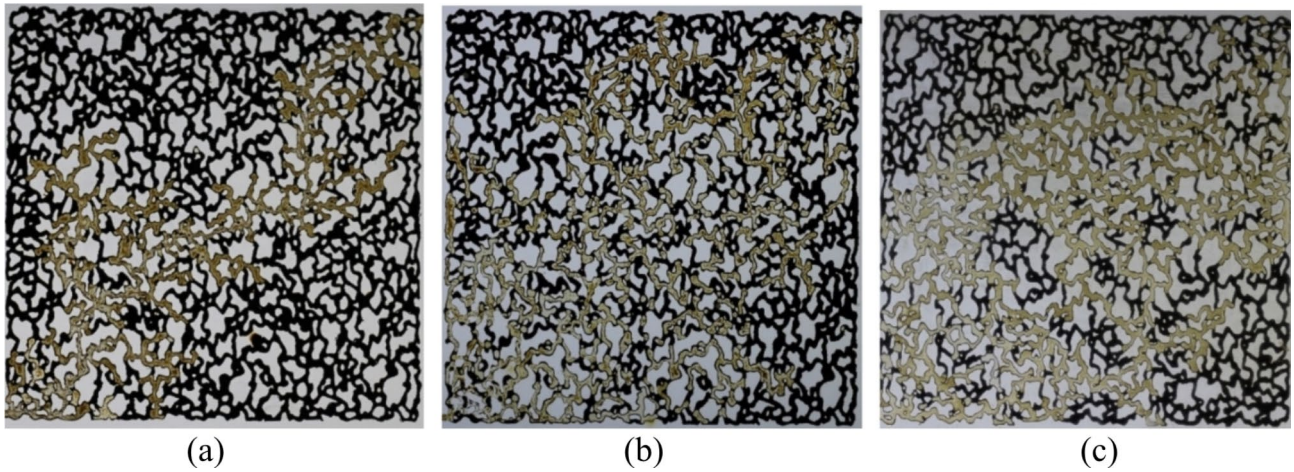

Fig. 18. Oil displacement during diluted seawater injection with biological zinc oxide NPs, (**a**) 0 ppm, (**b**) 500 ppm, (**c**) 1000 ppm.

Data availability

The datasets used and analysed during the current study available from the corresponding author on reasonable request.

Received: 10 September 2024; Accepted: 21 November 2024
Published online: 27 November 2024

References

1. Ying, S. et al. Green synthesis of nanoparticles: current developments and limitations. *Environ. Technol. Innov.* **26**, 102336. https://doi.org/10.1016/j.eti.2022.102336 (2022).
2. Ahmadi, Y., Sadeghi, Z., Kikhavani, T., Alibak, A. H. & Vaferi, B. Synthesis and application of eucalyptus plant-and walnut shell-CuO/Fe3O4/Xanthan polymeric nanocomposites for enhanced oil recovery in carbonate reservoirs. *J. Pet. Explor. Prod. Technol.* 1–10. https://doi.org/10.1007/s13202-024-01861-0 (2024).
3. Singh, J. et al. Green'synthesis of metals and their oxide nanoparticles: applications for environmental remediation. *J. Nanobiotechnol.* **16**, 1–24. https://doi.org/10.1186/s12951-018-0408-4 (2018).
4. Koopi, H. & Buazar, F. A novel one-pot biosynthesis of pure alpha aluminum oxide nanoparticles using the macroalgae Sargassum ilicifolium: a green marine approach. *Ceram. Int.* **44** (8), 8940–8945. https://doi.org/10.1016/j.ceramint.2018.02.091 (2018).
5. Chopra, H. et al. Green metallic nanoparticles: biosynthesis to applications. *Front. Bioeng. Biotechnol.* **10**, 874742. https://doi.org/10.3389/fbioe.2022.874742 (2022).
6. Hano, C. & Abbasi, B. H. Plant-based green synthesis of nanoparticles: production, characterization and applications. *Biomolecules* **12** (1), 31. https://doi.org/10.3390/biom12010031 (2021).
7. Sunkar, S. & Nachiyar, C. V. Biogenesis of antibacterial silver nanoparticles using the endophytic bacterium *Bacillus cereus* isolated from *Garcinia xanthochymus*. *Asian Pac. J. Trop. Biomed.* **2** (12), 953–959. https://doi.org/10.1016/S2221-1691(13)60006-4 (2012).
8. Pal, G., Rai, P. & Pandey, A. Green synthesis of nanoparticles: A greener approach for a cleaner future. In *Green Synthesis, Characterization and Applications of Nanoparticles* 1–26. https://doi.org/10.1016/B978-0-08-102579-6.00001-0 (Elsevier, 2019).
9. Huston, M., DeBella, M., DiBella, M. & Gupta, A. Green synthesis of nanomaterials. *Nanomaterials* **11** (8), 2130. https://doi.org/10.3390/nano11082130 (2021).
10. Zhang, Q. et al. Green-synthesized nickel oxide nanoparticles enhances biohydrogen production of Klebsiella sp. WL1316 using lignocellulosic hydrolysate and its regulatory mechanism. *Fuel* **305**, 121585. https://doi.org/10.1016/j.fuel.2021.121585 (2021).
11. Ghosh, S. et al. Mechanistic aspects of microbe-mediated nanoparticle synthesis. *Front. Microbiol.* **12**, 638068. https://doi.org/10.3389/fmicb.2021.638068 (2021).
12. Nagaraja, K., Hemalatha, D., Ansar, S. & Hwan, O. T. Novel, biosynthesis of palladium nanoparticles using strychnos potatorum polysaccharide as a green sustainable approach; and their effective catalytic hydrogenation of 4-nitrophenol. *Int. J. Biol. Macromol.* **253**, 126983. https://doi.org/10.1016/j.ijbiomac.2023.126983 (2023).
13. Koul, B., Poonia, A. K., Yadav, D. & Jin, J. O. Microbe-mediated biosynthesis of nanoparticles: applications and future prospects. *Biomolecules* **11** (6), 886. https://doi.org/10.3390/biom11060886 (2021).
14. Manivasagan, P. et al. Production of α-amylase for the biosynthesis of gold nanoparticles using Streptomyces sp. MBRC-82. *Int. J. Biol. Macromol.* **72**, 71–78. https://doi.org/10.1016/j.ijbiomac.2014.07.045 (2015).
15. Kalpana, V. N. et al. Biosynthesis of zinc oxide nanoparticles using culture filtrates of Aspergillus Niger: antimicrobial textiles and dye degradation studies. *OpenNano* **3**, 48–55. https://doi.org/10.1016/j.onano.2018.06.001 (2018).
16. Bandeira, M., Giovanela, M., Roesch-Ely, M. & Devine, D. M. & Da Silva Crespo, J. Green synthesis of zinc oxide nanoparticles: a review of the synthesis methodology and mechanism of formation. *Sustain. Chem. Pharm.* **15**, 100223. https://doi.org/10.1016/j.scp.2020.100223 (2020).
17. Tripathi, R. et al. ZnO nanoflowers: novel biogenic synthesis and enhanced photocatalytic activity. *J. Photochem. Photobiol. B.* **141**, 288–295. https://doi.org/10.1016/j.jphotobiol.2014.10.001 (2014).
18. Selvarajan, E. & Mohanasrinivasan, V. J. M. L. Biosynthesis and characterization of ZnO nanoparticles using Lactobacillus plantarum VITES07. *Mater. Lett.* **112**, 180–182. https://doi.org/10.1016/j.matlet.2013.09.020 (2013).
19. Libin, K. V., Sisodiya, S. & Debnath, M. Biosynthesis and antimicrobial activities of Tinospora cordifolia zinc nanoparticles. *Materi. Today Proc.* **79**, 367–374. https://doi.org/10.1016/j.matpr.2022.12.159 (2023).
20. Shanmugam, R. et al. Probiotic-bacteria (*Lactobacillus fermentum*)-wrapped zinc oxide nanoparticles: biosynthesis, characterization, and antibacterial activity. *Fermentation* **9** (5), 413. https://doi.org/10.3390/fermentation9050413 (2023).
21. Ahmadi, Y. et al. Application of green polymeric nanocomposites for enhanced oil recovery by spontaneous imbibition from carbonate reservoirs. *Polymers* **15** (14), 3064. https://doi.org/10.3390/polym15143064 (2023).
22. Sharma, P., Guha, A. & Das, S. Impact and challenges of nanotechnology in enhanced oil recovery. *Mater. Today Proc.* https://doi.org/10.1016/j.matpr.2023.05.655 (2023) (**in press**).
23. Wang, B. et al. Synthesis and enhanced oil recovery potential of the bio-nano-oil displacement system. *ACS Omega*. **8** (19), 17122–17133. https://doi.org/10.1021/acsomega.3c01447 (2023).
24. Sircar, A., Rayavarapu, K., Bist, N., Yadav, K. & Singh, S. Applications of nanoparticles in enhanced oil recovery. *Pet. Res.* **7** (1), 77–90. https://doi.org/10.1016/j.ptlrs.2021.08.004 (2022).
25. El-Masry, J. F., Bou-Hamdan, K. F., Abbas, A. H. & Martyushev, D. A. A comprehensive review on utilizing nanomaterials in enhanced oil recovery applications. *Energies* **16** (2), 691. https://doi.org/10.3390/en16020691 (2023).
26. Iravani, M., Khalilnezhad, Z. & Khalilnezhad, A. A review on application of nanoparticles for EOR purposes: history and current challenges. *J. Pet. Explor. Prod. Technol.* **13** (4), 959–994 (2023).
27. Mansouri, M., Ahmadi, Y., Sedghamiz, M. A. & Vaferi, B. Experimental investigation of the influence of ZnO–CuO nanocomposites on interfacial tension, contact angle, and oil recovery by spontaneous imbibition in carbonate rocks. *Phys. Fluids*. **36** (10). https://doi.org/10.1063/5.0231237 (2024).
28. Ahmadi, Y., Mansouri, M. & Pourafshary, P. Application of ZnO–TiO2/zeolite nanocomposites to enhance oil recovery from sandstone formations. *Pet. Sci. Technol.* 1–14. https://doi.org/10.1080/10916466.2023.2246491 (2023).
29. Lashari, N. & Ganat, T. Emerging applications of nanomaterials in chemical enhanced oil recovery: Progress and perspective. *Chin. J. Chem. Eng.* **28** (8), 1995–2009. https://doi.org/10.1016/j.cjche.2020.05.019 (2020).
30. Ahmadi, Y., Mansouri, M. & Pourafshary, P. Enhanced oil recovery by using modified ZnO nanocomposites in sandstone oil reservoirs. *Sci. Rep.* **14** (1), 2766. https://doi.org/10.1038/s41598-024-53138-5 (2024).
31. Ahmadi, Y. & Mansouri, M. Experimental optimization of activated carbon–zinc oxide for enhanced oil recovery in sandstone reservoirs. *Arab. J. Sci. Eng.* **48** (12), 17023–17030. https://doi.org/10.1007/s13369-023-08337-z (2023).
32. Soleimani, H. et al. Synthesis of ZnO nanoparticles for oil–water interfacial tension reduction in enhanced oil recovery. *Appl. Phys. A.* **124**, 1–13. https://doi.org/10.1007/s00339-017-1510-4 (2018).
33. Kadam, A. N. et al. Facile synthesis of Ag-ZnO core–shell nanostructures with enhanced photocatalytic activity. *J. Ind. Eng. Chem.* **61**, 78–86. https://doi.org/10.1016/j.jiec.2017.12.003 (2018).

34. Al-Naim, A. F., Sedky, A., Afify, N., Ibrahim, S. S. & Structural FTIR spectra and optical properties of pure and co-doped zn 1-x-y Fe x M y O ceramics with (M = Cu, Ni) for plastic deformation and optoelectronic applications. *Appl. Phys. A.* **127**, 1–20. https://doi.org/10.1007/s00339-021-04915-w (2021).
35. Talam, S., Karumuri, S. R. & Gunnam, N. Synthesis, characterization, and spectroscopic properties of ZnO nanoparticles. *Int. Sch. Res. Notices.* **1**, 372505. https://doi.org/10.5402/2012/372505 (2012).
36. Mohan, A. C. & Renjanadevi, B. J. P. T. Preparation of zinc oxide nanoparticles and its characterization using scanning electron microscopy (SEM) and X-ray diffraction (XRD). *Proc. Technol.* **24**, 761–766. https://doi.org/10.1016/j.protcy.2016.05.078 (2016).
37. Asadzadeh, N., Ahmadlouydarab, M. & Haddad, A. S. Effects of temperature and nanofluid type on the oil recovery from a vertical porous media in antigravity fluid injection. *Chem. Eng. Res. Des.* **193**, 394–408. https://doi.org/10.1016/j.cherd.2023.03.046 (2023).
38. Tadros, T. General principles of colloid stability and the role of surface forces. *Wiley-VCH: Weinheim.* **1**, 1–22. https://doi.org/10.1002/9783527631193 (2007).

Acknowledgements

The authors would like to thank Tarbiat Modares University and they would like to acknowledge the financial support of Ministry of Science, Research and Technology and Modares Science and Technology Park for this project under Grant number 02-00-02-001082. This study was financially supported by grant of the Nanotechnology and Biotechnology Development Councils of the Islamic Republic of Iran.

Author contributions

M.H.S.: Conceptualization, data curation, investigation, methodology, validation, writing—original draft. A.J.: Funding acquisition, project administration, resources, supervision, writing—review and editing. M.M.: Supervision, writing—review and editing. S.M.M.: Methodology, visualization, writing—review and editing.

Declarations

Competing interests

The authors declare no competing interests.

Additional information

Correspondence and requests for materials should be addressed to A.J. or M.M.